Chemistry–A European Journal
Research Article
doi.org/10.1002/chem.202202694
Chemistry Europe
European Chemical Societies Publishing
www.chemeurj.org

Ruthenium(II)-Dithiocarbazates as Anticancer Agents: Synthesis, Solution Behavior, and Mitochondria-Targeted Apoptotic Cell Death

Gurunath Sahu,[a] Sushree Aradhana Patra,[a] Sudhir Lima,[a, b] Sanchita Das,[a] Helmar Görls,[b] Winfried Plass,*[b] and Rupam Dinda*[a]

Abstract: The reaction of the $Ru(PPh_3)_3Cl_2$ with HL^{1-3}–OH (–OH stands for the oxime hydroxyl group; HL^1–OH = diacetylmonoxime-S-benzyldithiocarbazonate; HL^2–OH = diacetylmonoxime-S-(4-methyl)benzyldithiocarbazonate; and HL^3–OH = diacetylmonoxime-S-(4-chloro)benzyl-dithiocarbazonate) gives three new ruthenium complexes $[Ru^{II}(L^{1-3}–H)(PPh_3)_2Cl]$ (**1**–**3**) (–H stands for imine hydrogen) coordinated with dithiocarbazate imine as the final products. All ruthenium(II) complexes (**1**–**3**) have been characterized by elemental (CHNS) analyses, IR, UV-vis, NMR (^1H, ^{13}C, and ^{31}P) spectroscopy, HR-ESI-MS spectrometry and also, the structure of **1**–**2** was further confirmed by single crystal X-ray crystallography. The solution/aqueous stability, hydrophobicity, DNA interactions, and cell viability studies of **1**–**3** against HeLa, HT-29, and NIH-3T3 cell lines were performed. Cell viability results suggested **3** being the most cytotoxic of the series with IC_{50} 6.9 ± 0.2 μM against HeLa cells. Further, an apoptotic mechanism of cell death was confirmed by cell cycle analysis and Annexin V-FITC/PI double staining techniques. In this regard, the live cell confocal microscopy results revealed that compounds primarily target the mitochondria against HeLa, and HT-29 cell lines. Moreover, these ruthenium complexes elevate the ROS level by inducing mitochondria targeting apoptotic cell death.

Introduction

Ruthenium-based therapeutics of the platinum-group metals have been the focus of significant interest because of their acceptable biological and rich anticancer properties.[1] Platinum-based anticancer drugs such as cisplatin, oxaliplatin, and carboplatin are potent against a variety of cancerous cells, but the lack of selectivity, solubility, and other side effects have prompted researchers to develop anticancer agents that differ from the stereotypical ones.[2] Thus, there are multiple reports on ruthenium complexes that have been explored for anticancer studies within the frame of a possible "ruthenotherapy".[3] NAMI-A,[4] KP1019,[5] and its sodium salt analogue (N)KP-1339,[6] are the ruthenium complexes that have progressed into the human and clinical testing.[7] RAPTA is another Ru(II) complex that induces detachment from the primary tumor cell mass, migration and invasion, and activates mitochondrial apoptosis.[8] Both RM175 and ONCO4417 demonstrate apoptosis by causing cell death by G2/M phase arrest. ONCO4417 caused DNA damage at similar levels to cisplatin. (Figure 1).[9]

Besides the above ruthenium drugs, ruthenium-polypyridyl[1i,10] and ruthenium-arene[11] complexes have also been reported extensively as potential chemotherapeutic agents. In spite of these ruthenium complexes, there may still be new opportunities for developing anticancer agents based

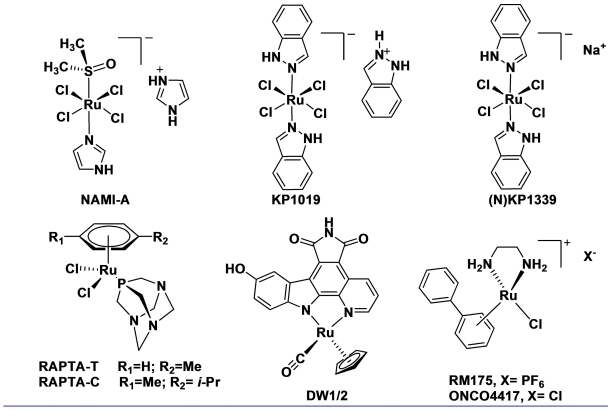

Figure 1. Structures of ruthenium compounds in clinical, and preclinical trials.

[a] G. Sahu, S. A. Patra, S. Lima, S. Das, Prof. Dr. R. Dinda
Department of Chemistry
National Institute of Technology
Rourkela 769008, Odisha (India)
E-mail: rupamdinda@nitrkl.ac.in
[b] S. Lima, Dr. H. Görls, Prof. Dr. W. Plass
Institut für Anorganische und Analytische Chemie
Friedrich-Schiller-Universität Jena
Humboldtstr. 8, 07743 Jena (Germany)
E-mail: sekr.plass@uni-jena.de

Supporting information for this article is available on the WWW under https://doi.org/10.1002/chem.202202694

on ruthenium systems incorporated with some other bioactive ligands.

In the development of anticancer agents, ligand design is extremely important. In medicinal chemistry, dithiocarbazate Schiff-base derivatives of S-alkyl and S-aryl groups are emerging ligands with various pharmaceutical and biological properties, such as anticancer, antiamoebic, and antibacterial properties.[12] Like thiosemicarbazones, they possess NS-donors, enclosed in a thioamide moiety (thione-thiol). In recent times, *in vitro* tests have shown some promising anticancer activity of non-Pt-metallic complexes with dithiocarbamate Schiff-base ligands.[13] These ligands have a vital role in cytotoxicity against the human pancreatic cell lines namely, PANC-1, ASPC-1, and BxPc-3 as reported by Gou et al.[14] during the investigation of a series of fluorescent dithiocarbazate based Fe(II), Co(II), Ni(II), Cu(II), and Zn(II) complexes. Their complexes also displayed anticancer activity against a pancreatic cancer xenograft in mice with low toxicity. Thus, dithiocarbazate Schiff-base ligands containing non-Pt-metal complexes offer great potential as anticancer agents.

Furthermore, metal complexes coordinated with triphenylphosphine (PPh_3) also have pharmacophoric interest as they exhibit fluorescent properties that provide valuable information about the distribution, absorption, and uptake of anticancer drugs in living cells and are also excellent for chemotherapy since they influence mitochondrial activity.[15] As a result of their increased membrane crossing property,[15b,16] hydrophobic PPh_3 ligated systems have good cytotoxicity. Dithiocarbazate derivatives and PPh_3 derivative complexes are therefore cytotoxic and have drawn our attention to investigate new mixed dithiocarbazate based Schiff base and PPh_3 coordinated complexes. In recent times, two azo and PPh_3 derived mixed ligand ruthenium(II) complexes have been reported by us exhibiting impressive cytotoxicity against both HeLa and HT-29 cancer cell lines (IC_{50} values between 3.84 and 4.48 μM).[16] Significant *in vitro* cytotoxic results of dithiocarbazate Schiff-base-vanadium complexes have also been reported in our very recent works,[17] which overall further stimulates us to design and investigate some fluorescent active PPh_3-coordinated Ru(II)-dithiocarbazate complexes (being non-polypyridyl-ruthenium and arene-ruthenium complex) to study their anticancer activity.

DNA is an important target for the transition metal-based anticancer drugs.[7,10c,11c,18] Metallodrugs usually damage the DNA or disrupt the DNA repair process in cancer cells by preventing cell division and triggering cancer cell apoptosis.[7,10e,11l] Literature suggests that ruthenium complexes with higher DNA binding affinity seem to enhance the anticancer activity; some polypyridyl or arene-based Ru(II) complexes were reported to exhibit the anticancer activity in parallel with their ability to interact with DNA.[7,10c,e,g,11c] However, in addition to DNA interaction, the cytotoxicity of Ru(II) compounds may attribute to other factors such as mitochondria-targeted apoptotic cell death via generation of reactive oxygen species (ROS) in tumor cells by targeting different mitochondrial enzymes.[10c,19] Few recent studies suggested that lipophilic Ru(II) complexes target the mitochondria and promote apoptosis by disturbing the mitochondrial membrane potential in cells.[20] Thus, it is an important aspect to investigate the hydrophobicity, DNA interaction, and also intracellular target of the complexes in the motif of cytotoxicity studies.

Based on these factors and our past experiences with transition metals in anticancer studies,[16,17,21] three new compounds of ruthenium(II)-4-R-aroyldithiocarbazoneimine have been synthesized and characterized by various physicochemical techniques including the structure of **1**, and **2** solved by single crystal X-ray analysis. Here, three 4-R-aroyldithiocarbazoneoximes (Scheme 1) were used as ligands, each with a different inductive effect (R=H, Me, and Cl), in order to examine their effects, if any, on the biological activity of the complexes.[22] The hydrophobicity of **1**–**3** was tested by partition coefficient measurements (log P_{ow}). The interaction of the complexes with calf thymus (CT) DNA was studied by UV-vis absorption titration and fluorescence quenching experiments. Finally, the *in vitro* cytotoxicity of **1**–**3** was tested against cancerous HeLa, and HT-29, and the noncancerous NIH-3T3 cell lines. The apoptotic pathway was tested by cell cycle arrest and Annexin V-FITC/Propidium Iodide (PI) assays. Compounds being highly cytotoxic, the intracellular target and apoptotic mode of complexes were investigated through confocal microscopy and ROS (reactive oxygen species) analysis. It is the first detailed study, to the best of our knowledge, to evaluate the effects of Ru(II)-dithiocarbazate complexes on cancer cells, where all complexes cause apoptosis via mitochondrial dysfunction. Overall, this study shows the success of mitochondria-targeted ruthenium-aroyldithiocarbazoneimine complexes as successful luminescent anticancer agents.

Results and Discussion

Synthesis and Characterization

Refluxing an equimolar ratio of HL^{1-3}–OH, with $[Ru(PPh_3)_3Cl_2]$ in ethanol under normal atmospheric conditions, afforded $[Ru^{II}(L^{1-3}–H)(PPh_3)_2Cl]$ (**1**–**3**), respectively (Scheme 1). Initial characterizing tools such as elemental (C, H, and N) analyses, IR, NMR, UV-vis, and HR-ESI-MS identified the formation of the com-

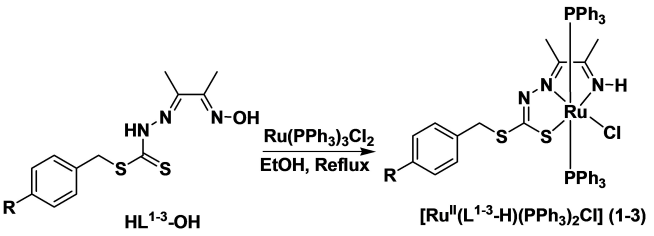

R	Ligand	Complex
H	HL^1-OH	1
Me	HL^2-OH	2
Cl	HL^3-OH	3

Scheme 1. Preparation routes of $[Ru^{II}(L^{1-3}–H)(PPh_3)_2Cl]$ (**1**–**3**).

plexes, and the occurrence was further confirmed by X-ray crystallography.

All complexes undergo an *in situ* ruthenium-assisted organic transformation of the oxime to imine during metalation.[23] The spontaneous oxygen atom transfer processes involved in dithiocarbazate oxime ligands to their corresponding metal coordinated dithiocarbazate imine species were investigated with a proposed mechanism (Eq. (1), Scheme 2). During the course of the reaction of $Ru(PPh_3)_3Cl_2$ and HL^{1-3}–OH, an oxygen atom from the oxime ligand has been transferred to a PPh_3, dissociated from $[Ru(PPh_3)_3Cl_2]$, and forms an imine ligand coordinated ruthenium(II) complexes $[Ru^{II}(L^{1-3}–H)(PPh_3)_2Cl]$ (**1**–**3**) along with $OPPh_3$ elimination.[23a,24] Also, to establish this as a metal(Ru)-assisted transformation we carried out similar reactions using free PPh_3 and also other metal precursor like $[Ir(PPh_3)_3Cl]$. However, no evidence of oxime to imine transformations was observed[23a] (Figure S1).

$$[Ru^{II}(PPh_3)_3Cl_2] + HL^{1-3}\text{-}OH \longrightarrow [Ru^{II}(PPh_3)_2Cl(L^{1-3}\text{-}H)] + OPPh_3 + HCl \quad (1)$$

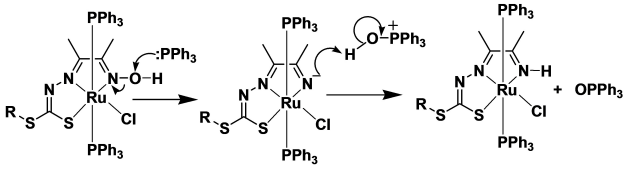

Scheme 2. Proposed mechanisms for the formation of $[Ru(PPh_3)_2(L^{1-3}–H)Cl]$ (**1**–**3**) [R = benzyl for **1**; 4-methylbenzyl for **2**; and 4-chlorobenzyl for **3**].

IR Spectroscopy

The infrared spectra of HL^{1-3}–OH and **1**–**3** are performed and the results are added in the *experimental section*. **1**–**3** exhibit some bands at ~515, 695, and 745 cm^{-1} for ν(P–C) bonds of triphenylphosphine molecule and at ~330 cm^{-1} due to the ν(Ru–Cl) fragment coordinated to the metal centre.[16,23a] Further, a stretching band near ~3450 cm^{-1} may be assigned to the $\nu(N–H)_{imine}$ in all three complexes.[23a,24] By using solution FTIR (Figure 2), $OPPh_3$, produced during the synthesis of the complexes, was identified (νP=O observed at 1192 cm^{-1})[24] in the filtrate residue of **1** taking as representative.

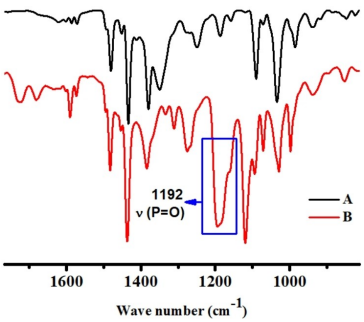

Figure 2. IR spectra of A) Pure crystals; B) Filtrate residue of **1**.

X-ray Crystallography of 1–2

Two structures, $[Ru^{II}(L^{1}–H)(PPh_3)_2Cl]$ (**1**), $[Ru^{II}(L^{2}–H)(PPh_3)_2Cl]$ (**2**), were studied with the help of crystallographic technique. The ORTEP diagrams are depicted in Figure 3, whereas relevant crystallographic parameters are given in Table S1 and selected bond lengths and angles with estimated standard deviations are presented in Table 1. The X-ray structures can be best described as distorted octahedral with $Ru^{II}N_2P_2SCl$ geometry for metal centers **1**–**2** (See Figure 3). The ruthenium (II) species are coordinated in an N, N, and S tri-dentate mode by the uni-negative fashion. Out of the three remaining positions, the -Cl atom is present within the molecular plane whereas the other two are occupied by the PPh_3 groups present in axial positions to the molecular plane and are mutually trans to each other. The Ru–P bond lengths are lengthened (nearly 2.3621 Å) in the

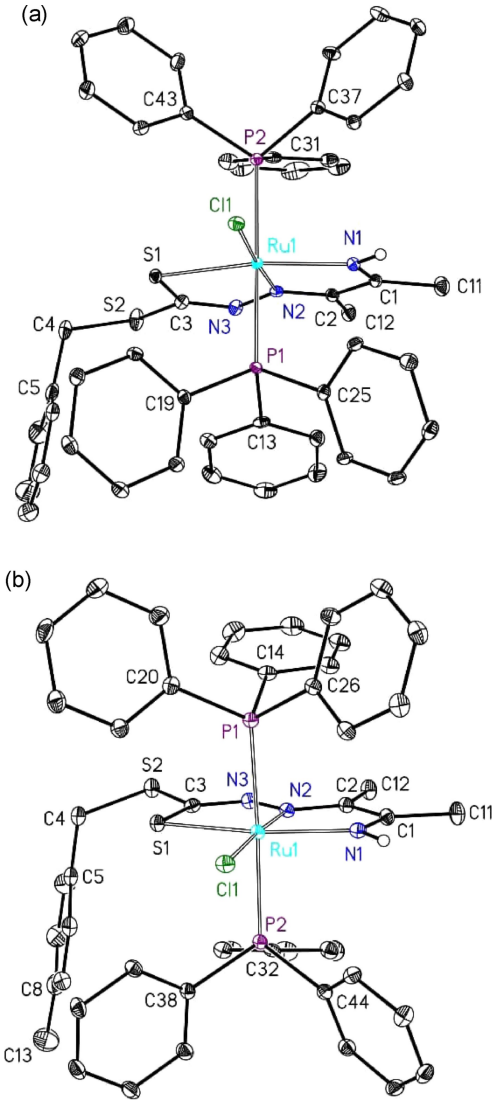

Figure 3. Molecular structures and selected atom numbering schemes of **1** (top) and **2** (bottom). The ellipsoids represent a probability of 30%, and H atoms bonded to N1 are drawn with arbitrary radii. All other Hydrogen atoms are omitted for clarity.

Table 1. Selected bond distances and angles for the ruthenium coordination of **1**–**2**.

	Bond lengths [Å]	
	1	**2**
Ru1–N2	l.969(3)	1.9722(19)
Ru1–N1	2.079(3)	2.074(2)
Ru1–P1	2.3638(8)	2.3651(6)
Ru1–P2	2.3730(8)	2.3754(6)
Ru1–S1	2.3953(8)	2.3904(6)
Ru1–Cl3	2.4773(8)	2.4743(6)
Bond angles (°)		
N2–Rul–Nl	77.01(11)	76.91(8)
N2–Rul–Pl	92.34(8)	91.80(6)
Nl–Rul–Pl	89.86(8)	90.99(6)
N2–Rul–P2	93.21(8)	92.70(6)
Nl–Rul–P2	90.59(8)	90.78(6)
Pl–Rul–P2	174.39(3)	175.43(2)
N2–Rul–Sl	81.99(8)	82.19(6)
Nl–Rul–Sl	158.99(8)	159.09(6)
Pl–Rul–Sl	90.48(3)	89.79(2)
P2–Rul–Sl	91.10(3)	90.05(2)
N2–Rul–Cl1	176.54(8)	175.77(6)
Nl–Rul–Cl1	99.53(8)	98.89(6)
Pl–Rul–Cl1	87.65(3)	87.76(2)
P2–Rul–Cl1	86.77(3)	87.80(2)
Sl–Rul–Cl1	101.47(3)	102.02(2)

axial positions due to the bulkier triphenylphosphine group whereas Ru–Cl is found to be ~2.47 Å. The observed Ru1–S1, Ru1–N1, Ru1–N2, Ru1–Cl1, Ru1–P1, and Ru1–P1 bond lengths are comparable with complexes reported in the literature.[23b] The ligand molecule with the metal center possesses two five-membered rings i.e. with RuN_2C_2 ring through an angle ∠N2–Ru1–N1 [77.01(11)°, **1**; and 76.91(8)°, **2**] and $RuSN_2C$ rings through an angle ∠N2-Ru1-S1 [81.99(8)°, **1**; and 82.19(6)°, **2**]. Considering the conversion of oxime to imine groups, it can be confirmed by bond parameters obtained by X-ray analysis for N1–H1 bond distances 0.85 Å for **1**, and 0.87 Å for **2** comparable to normal N–H bond distances reported earlier.[23–25] It is noteworthy that the Ru1–N2 bonds (1.969 Å, **1**; 1.972 Å, **2**) are shorter than the Ru1–N1 bonds (2.079 Å, **1**; 2.074 Å, **2**), indicating weak donor ability of the imine nitrogen group.[23b,25] As result, C2–N2 [1.321(4) Å, **1**; and 1.316(3) Å, **2**] were observed to be longer than that of the C1–N1 [1.302(4) Å, **1**; and 1.298(3) Å, **2**] bonds. Overall, the terminal M–L bonds [Ru1–N1, and Ru1–S1] were found to be longer than that of the central donor bond [Ru1–N2] of the tridentate ligand which is in agreement with earlier reports.[26]

Stability Studies in Solution/Aqueous Media

UV-vis Spectroscopy

The electronic spectra of **1**–**3** were recorded in the DMSO solution. The strong transitions in the range 350–360 nm of **1**–**3** are assigned to intra-ligand charge transfer transitions while the weaker transitions in the range 460–480 nm of the spectra are probably due to metal to ligand charge transfer transition (MLCT).[16,20] Representative UV-vis spectra of **1**–**3** are shown in Figure S2.

The stabilities of **1**–**3** were examined through two independent experiments under physiological conditions (H_2O, and DMEM solutions) at 298 K with the help of UV-vis spectroscopy. As shown in Figure S3, the absorbance of complexes was tested with an increase in the percentage of H_2O (up to 99% H_2O/1% DMSO v/v) by keeping the concentration of **1**–**3** at 1×10^{-4} M. From the results, complexes were found stable, and also no additional transitions were found in the absorbance spectra even in presence of excess H_2O. The time-dependent absorbance spectra (Figure S4) of each complex were also performed in 2:1 DMEM:DMSO (v/v) at different time intervals (0, 12, 24, and 48 h). The overall results indicated that there are no noticeable changes in the absorption spectra of **1**–**3** in presence of aqueous/biological media in the mentioned time period.

NMR Spectroscopy

^{1}H NMR spectra of HL^{1-3}–OH have been recorded in DMSO-d_6 whereas **1**–**3** in $CDCl_3$ and are depicted in Figures S5–S10 in Supporting Information. The ^{1}H and ^{13}C{H} NMR spectral data (added in the experimental section) of all the compounds are in accordance with their corresponding compositions. The imine N–H proton is observed at 8.41 ppm as a singlet peak suggesting the imine form of the ruthenium complexes.[24] Also, the ^{31}P NMR data of **1**–**3** exhibits a single peak at ~29 ppm can be assigned to the presence of the –PPh_3 group in the complex.[16] The detection of $OPPh_3$ isolated from the filtrate residue (**1**) was identified by solution ^{31}P NMR (δ 29.4 ppm) (Figure 4a).[24]

HR-ESI-MS

Masses of **1**–**3** have been performed in aqueous mixture solvents (H_2O, DMSO, and CH_3CN) in positive ion mode. The HR-ESI-MS shows the molecular ion peaks $[M]^+$ at $m/z = 925.1205$ for **1**, $m/z = 939.0727$ for **2**, and $m/z = 959.0744$ for **3**. In addition to the molecular ion peaks, some common solvent coordinated masses have also been observed for all three complexes. Overall, ruthenium metal remained intact with the ligands even in the presence of water which indicates that **1**–**3** is stable in the aqueous medium. A representative mass spectrum of **1** is shown in Figure 5, along with the detailed analysis of **1**–**3** has been added in Supporting Information (Figure S11–S13, Table S2–S4). The detection of $OPPh_3$ isolated from the filtrate residue (**1**) was also identified by HR-ESI-MS (m/z 279.1210; $OPPh_3 + H^+$) (Figure 4b).[24]

Partition Coefficients Measurements (log P_{ow})

Partition coefficients, log P_{ow}, were measured to establish a possible relationship between the hydrophobicity/lipophilicity and biological activity of the compounds.[21d,27] It has been

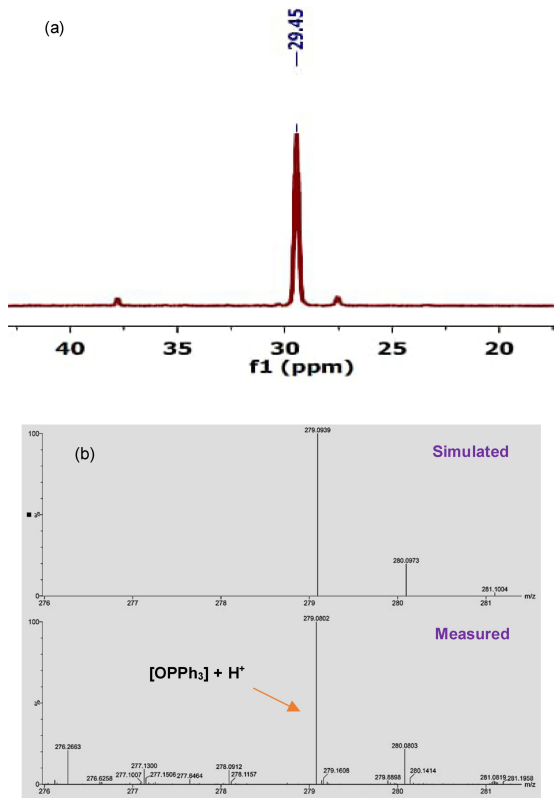

Figure 4. a) Detection of $OPPh_3$ in the filtrate of **1** by ^{31}P NMR; **b)** Detection of $OPPh_3$ in the filtrate of **1** by HR-ESI-MS.

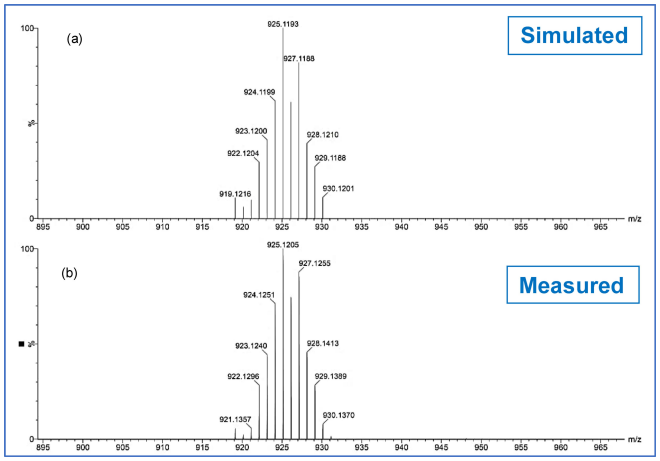

Figure 5. HR-ESI-MS spectrum of $[Ru(L^1–H)(PPh_3)_2Cl]$ (**1**) recorded in $H_2O:CH_3CN$ (10:90 v/v) in positive ion mode with (a) simulated and (b) observed isotopic distributions.

reported that hydrophobic cations have a higher affinity to accumulate in mitochondria due to the negative potential difference across the mitochondrial membrane.[20,28] Generally, the values of log P_{ow} range between −3 (very hydrophilic) to +10 (extremely hydrophobic).[21d] In this work, the observed log P_{ow} values (Table 2) are found 1.45 for **1**; 1.47 for **2**; and 1.63 for **3** by following the order **1** < **2** < **3**; with **3** being the most hydrophobic compound of the series. The positive log P_{ow} values of **1**–**3** suggest that all complexes are hydrophobic, perhaps because of triphenylphosphine groups present in the complex environment.[3a] Further, the high hydrophobicity of complex **3** (log P_{ow} = 1.63) may be due to the additional electron-withdrawing group present at the para position of the ligand moiety.[29]

DNA-Binding Assays

UV-vis spectroscopy titration is a frequently used technique for investigating the probable binding modes of complexes to CT-DNA and determining their binding constants (K_b).[30] So, here the binding of **1**–**3** with CT-DNA was performed through UV-vis spectroscopy. The extent of hypochromism/hyperchromism depends upon the binding affinity and mode of the complexes toward DNA. The DNA sample was sequentially added in aliquots (5 μM), and the absorbance were measured after each addition. The variations in the absorbance of **1**–**3** are presented in Figures 6 and S14. On gradual addition of CT-DNA, substantial decreases in the absorbance (hypochromic shift) at 370–380 nm are observed.

The calculated K_b ranged from 4.43×10^4 to 1.16×10^5 M^{-1}, increased order as follows **1** < **2** < **3**, suggesting that **3** has maximum interaction towards CT-DNA. Also, the binding activity of HL^{1-3}–OH was assayed and among the three ligands, HL^3–OH showed the maximum binding constant at 2.33×10^4 M^{-1}. However, as discussed above the actual ligands have been transformed into their corresponding imine species during the metalation reaction. Therefore, the results suggest that the

Table 2. Partition coefficients (log P_{ow}) of **1**–**3**.

Complex	Partition coefficient (log P_{ow})
1	1.45
2	1.47
3	1.63

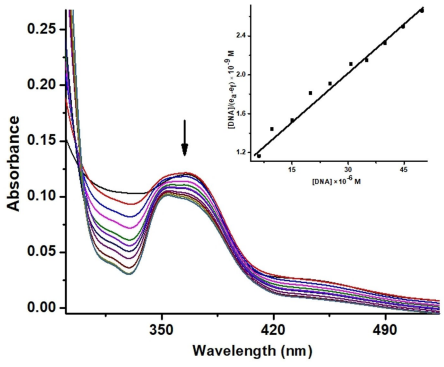

Figure 6. Absorption spectra of **1** in 50 mM Tris–HCl buffer (pH = 7.4), 298 K in the presence of increasing amounts of CT-DNA. [Ru] = 10 μM, [CT-DNA] = 0-50 μM from top to bottom. Arrows indicate the change in absorbance upon increasing the DNA concentration. Inset shows a linear fit plot of $[DNA]/(\varepsilon_a-\varepsilon_f)$ vs. [DNA].

better binding of **3** may be due to the presence of a chlorine atom at the para position which may slightly shift the dipole of the molecule at the binding site, for enhanced interaction with CT-DNA.[22b,31] Another probable reason is that the presence of chlorine substituents in complexes/ligands may change their ability to strongly bind to CT-DNA by increasing their hydrophobic properties.[22b,29,31] In agreement with the preliminary studies, the extent of intercalation was further investigated using EB displacement studies.

Competitive DNA Binding Assays

Ethidium bromide (EB) is an effective fluorescent tool that binds to DNA through intercalation mode. EB (black spectral line in Figure 7a) upon binding with CT-DNA gets fluorescent active (can be seen as a red spectral line in Figure 7a). As shown in Figures 7 and S15, with the gradual addition of complexes to luminescent EB-DNA adduct the emission intensity was quenched significantly leading to the displacement of bound EB from the adduct. As a result, the K_{sv} values of **1**–**3** for EB-bound CT-DNA complexes are found in the range 1.49×10^4 to 1.79×10^4 M^{-1} whereas the binding constant (K_b) in the range 8.29×10^4 to 1.31×10^5 M^{-1}, with order **1** < **2** < **3**. A higher K_b value of 1.31×10^5 M^{-1} for complex **3** indicates better intercalation with CT-DNA.

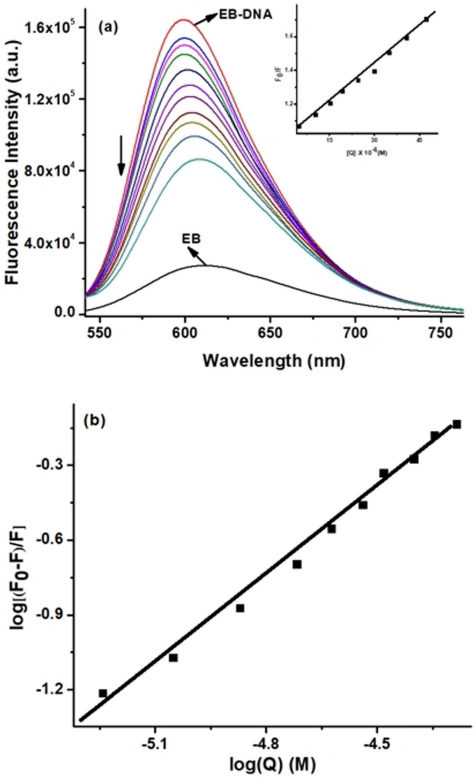

Figure 7. (a) Fluorescence titration of the EB bound CT-DNA by increasing concentrations of **1** (5–50 μM) (λ_{ex} 520 nm; λ_{em} 530–800 nm) with insets showing the Stern–Volmer plot for the quenching of fluorescence intensity on the addition of the ruthenium complex. (b) Scatchard plot of complex **1**.

Circular Dichroism (CD) Analysis with CT-DNA

CD is a powerful tool used to diagnose the conformational changes in DNA helix in order to elucidate the groove and intercalation binding of the complexes.[21k,32] During groove or electrostatic interaction with CT-DNA, the intrinsic CD spectra are less or not perturbed, whereas during intercalation there is an increase in the intensity of both negative and positive bands.[21k,32] It was observed that (Figure 8) both negative (helicity) and positive (ellipticity) bands increased significantly after complexes **1**–**3** were treated with CT-DNA, further suggesting intercalation binding.

Cytotoxicity

The *in vitro* cytotoxicity of HL^{1-3}–OH, and $[Ru^{II}(L^{1-3}–H)(PPh_3)_2Cl]$ (**1**–**3**) was evaluated using standard MTT assays against two cancer cell line, i.e., human cervical cancer (HeLa), and human colon cancer (HT-29). The IC_{50} values of **1**–**3** are found in the ranges of 6.9–12.1 and 13.9–32.8 μM against HeLa and HT-29 cells, respectively (Table 3, Figure 9, and Figure S16–S17). The cytotoxicity increased with compound order **1** < **2** < **3** and compound **3** was the most toxic with IC_{50} values of 6.9 ± 0.2 μM against HeLa, and 13.9 ± 0.4 μM against HT-29 cell lines. An analogous trend is observed in the cell-specific selectivity of **1**–**3** against both cell lines. The results revealed that **1**–**3** exerts

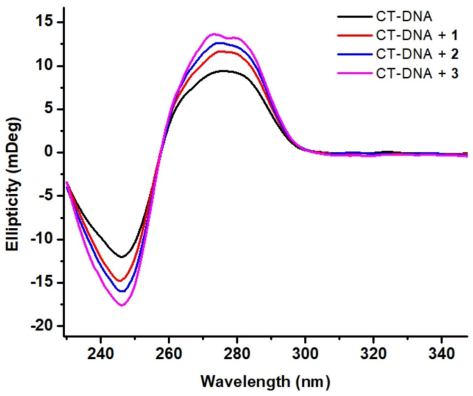

Figure 8. CD spectra of CT-DNA (150 μM) in the presence and absence of **1**–**3** in 50 mM Tris–HCl buffer (pH 7.4). The path length of the cuvette was 5 mm.

Table 3. Effect of complexes (**1**-**3**) against HeLa, HT-29, and NIH-3T3 cells. IC_{50} values were perceived by the MTT assay, post 48 h incubation.

Complex	IC_{50} [μM] HeLa	HT-29	NIH-3T3
1	12.1 ± 0.1	32.8 ± 0.4	46.1 ± 1.4
2	7.8 ± 0.1	24.5 ± 0.1	23.4 ± 0.5
3	6.9 ± 0.2	13.9 ± 0.4	36.7 ± 0.1
HL^1–OH	>50	31.4 ± 1.6	>50
HL^2–OH	31.8 ± 2.7	28.5 ± 0.1	35.8 ± 0.9
HL^3–OH	25.7 ± 4.6	11.8 ± 0.3	>50
Cisplatin	25.5 ± 0.8	32.7 ± 0.6	–

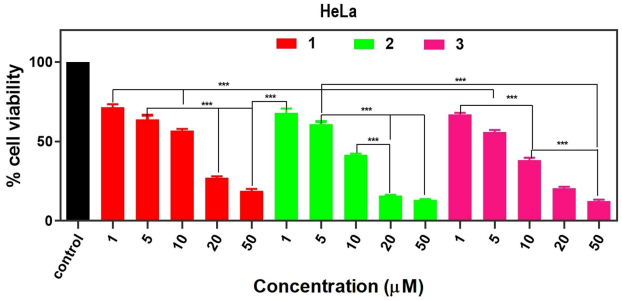

Figure 9. *In vitro* cytotoxicity profile of the tested complexes (**1**-**3**) against HeLa cell line after 48 h incubation. Data are reported as the mean ± SD for n = 4 and ***p < 0.0001.

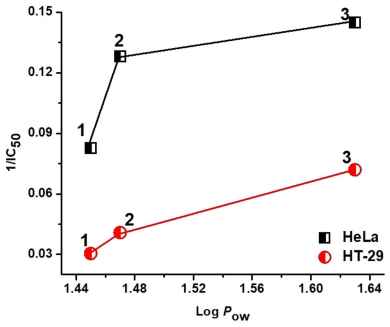

Figure 10. Correlation between cytotoxicity (HeLa and HT-29) and partition coefficient (log P_{ow}).

effective toxicity in inhibiting the growth of cancer cells and were highly toxic even at lower concentrations. At their highest dose (50 μM), almost 80% cell inhibition was seen (Figure 9 and S16–S17) after 48 h of exposure.

Again, to determine the degree of selectivity on cancerous cells, the cytotoxicity of investigated molecules was also evaluated against noncancerous cells NIH-3T3. According to the results (Table 3), complexes were less toxic to normal cells, NIH-3T3 with IC_{50} values in the range of 36.7 to 46.1 μM. In the present study, **3** with a selectivity index (SI) of 5.3 folds was chosen as the most promising anticancer compound for HeLa cells.

As mentioned earlier, dithiocarbazate-based ligands also exhibited significant cytotoxicity.[12g–h,14] In fact, HL^3–OH with IC_{50} 11.8 ± 0.3 μM showed better toxicity (Table 3) than metal complexes (**1**–**3**) against HT-29 cells; to be precise, the better cytotoxicity of HL^3–OH and **3** may be due to the effect of the chlorine group present at the para position of ligand molecule.[22b–d] Further, from ESI-MS results some solvent coordinated ruthenium species are also observed (*see HR-ESI-MS section*), so the overall cytotoxicity perceived from individual compounds may be originated from all the possible mixture species generated in the incubation media.[17a,21a–b]

In addition, lipophilicity is a vital property of compounds that is directly related to anticancer activity as it allows a compound to diffuse through the biological lipid layer leading to better availability of compounds in its target, and also useful to the maximum cellular uptake of complexes leading to better cytotoxicity activity.[21d,27,29,33] Based on the results of log P_{ow} (Table 2), and IC_{50} values (Table 3), complexes with high hydrophobic behavior induced maximum effect on anticancer activity. As presented in Figure 10, with the increase in the hydrophobicity of **1**–**3**, an increase in cytotoxicity activities (IC_{50}) was observed. Overall, it can be concluded that, the compound (**1**-**3**) with higher hydrophobicity and stronger DNA interaction (as discussed in the DNA binding section above) has shown better anticancer activity.[18,20,21d,34]

Nonetheless, under similar conditions, **1**–**3** show comparable anticancer activity with respect to the existing chemotherapeutic drug cisplatin (25.5 ± 0.8 and 32.7 ± 0.6 μM against HeLa and HT-29, respectively See Table 3). Moreover, the above *in vitro* cytotoxicity results of **1**–**3** are better than or comparable with those of other ruthenium-dithiocarbazate species [Ru(H-Nap-sbdtc)$(PPh_3)_2$(CO)Cl] and [Ru(H-Nap-sbdtc)$(AsPh_3)_2$(CO)–Cl] (IC_{50} between 22.9 to 26.4 μM against HeLa cells);[12i] ruthenium-arene species [$(\eta^6$-p-cym)Ru(NN)Cl]PF_6 (IC_{50} > 100 μM against HeLa cells);[35] and Keppler-type ruthenium-trifluoromethyl species Na[$RuCl_4(CF_3Hin)_2$] and Na[$RuCl_4(CF_3Him)_2$] (IC_{50} > 24-100 μM against HT-29 cells).[36]

According to the results of all the investigated compounds, complex **3** exhibited the maximum anticancer activity against HeLa cells. Cancer cell proliferation may be inhibited by **3** through induction of either apoptosis or cell cycle arrest, or by a combination of both. In order to examine the mode of cell death induced by these complexes, flow cytometric analysis with propidium iodide (PI) and Annexin V-FITC/PI was performed taking **3** as representatives.

Cell Cycle Analysis

Cell cycle arrest determines the effectiveness of an anticancer drug in stopping cancerous cell division.[35,37] The percentage of accumulation of HeLa cells after treatment at different concentrations (0.5 × IC_{50}, 1.0 × IC_{50}, 2.0 × IC_{50}) of **3** (the concentrations were taken after performing the MTT assay against HeLa cells for 24 h (Figure S18)) for 24 h in Sub-G0/G1, G0/G1, S, and G2/M has been shown in Figure 11. From the results, the number of cells in the Sub G0/G1 phase is increased with an increase in doses of **3** from 4.7% (untreated cells) to 9.0, 10.6, and 15.1%, respectively; along with in the S phase there is a straight increase from 14.3% (untreated cells) to 19.1, 19.4, and 25.2%, respectively. However, the G0/G1 phase is decreased from 57.9% (untreated cells) to 40.1% (at the highest concentration i.e. 2 × IC_{50}), whereas in G2/M no significant change is observed. These results indicated that complex **3** mainly arrested the S phase in a concentration dependent manner. Thus, the overall increase of the DNA content in Sub G0/G1 (sub-diploid) and S phase cells might result in apoptosis by disrupting the cell cycle.[35,38] Overall, the treatment of HeLa cells with **3** for 24 h resulted in a noticeable increase in the proportion of apoptotic cells in dose-dependent manner, as shown in the subdiploid region. Induction of apoptosis was further confirmed by Annexin V-FITC/PI apoptosis assay.

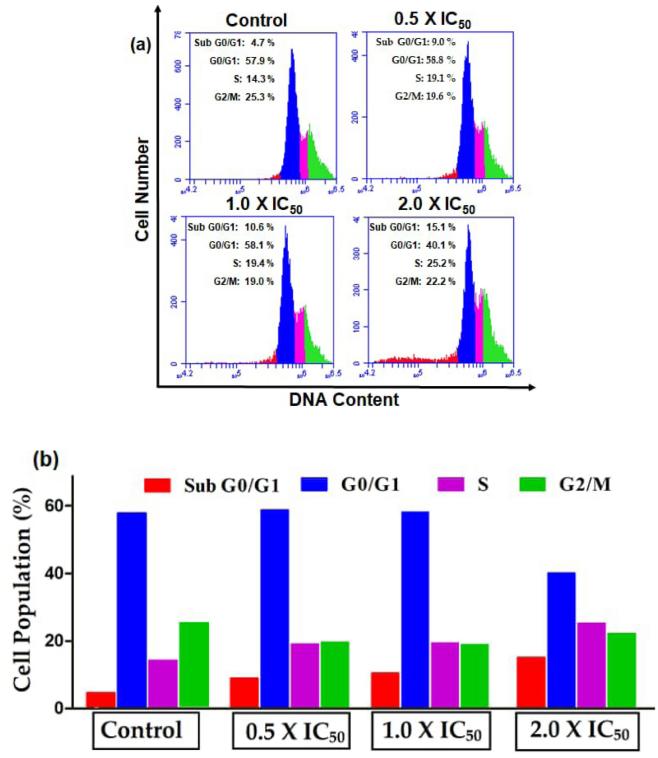

Figure 11. (a) Cell cycle analysis of HeLa cancer cells post treatment of **3** for 24 h. Cell staining for flow cytometry was performed using PI/RNase. (b) Histogram of the cell cycle distribution.

Double-Staining Apoptosis Assay

An Annexin V-FITC/propidium iodide (PI) measurement is required to determine whether the complex induces cell death through apoptosis or necrosis. So, the HeLa cells were stained with Annexin V-FITC/PI reagents, and apoptosis was analyzed using a flow cytometer. The different stages of cells, i.e., live cells, early apoptotic cells, late apoptotic cells, and necrotic were calculated using the fluorescence-activated cell sorting (FACS) methodology. So, at three different concentrations (0.5× IC_{50}, 1.0×IC_{50}, and 2.0×IC_{50},) of complex **3**, the cell population in the lower right quadrant represents cells undergoing early apoptosis, which increased from 4.5% (Control) to 27.8, 36.1 and 41.3% with an increase in concentrations of **3**, respectively (Figure 12). However, no significant cell population was observed in the late apoptotic and necrotic regions. Altogether, the flow cytometry result concluded that the cell death induced by **3** is mainly caused by apoptosis. (Figure 12) Further, the effect of ROS on apoptosis induced by **3**, was investigated in presence of ROS scavenger *N*-acetylcysteine (NAC) before being treated with the complex.[39] As shown in Figure 12c, about a 26% decrease in the apoptotic cells indicates that ROS plays a crucial role in cell apoptosis.

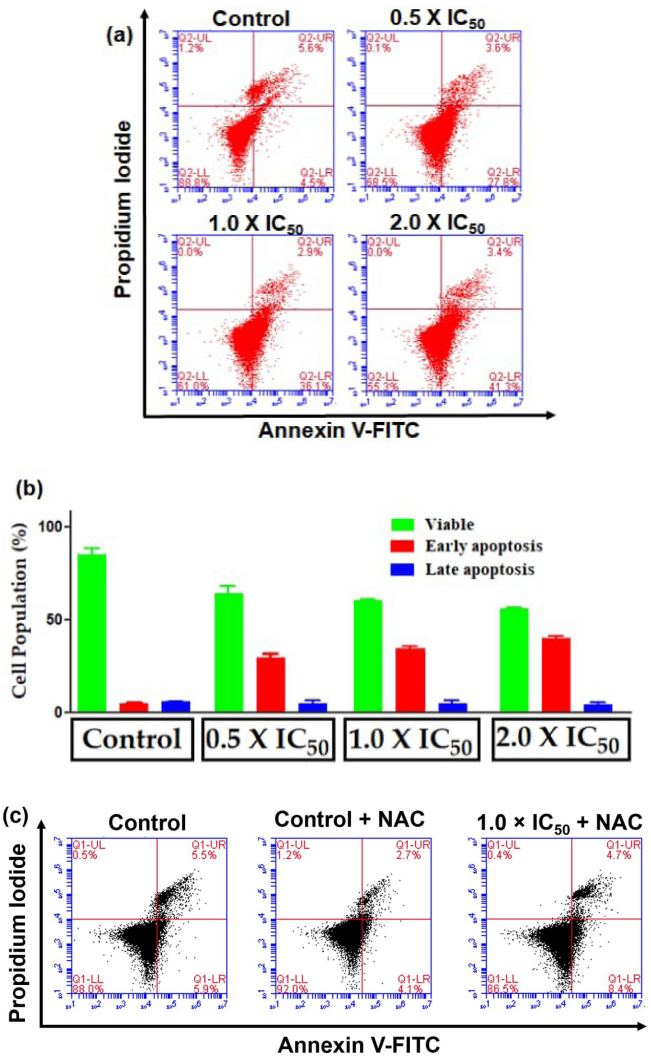

Figure 12. a) Induced apoptosis in HeLa cells upon treatment of three different concentrations of **3** for 24 h measured by flow cytometer using Annexin V-FITC/propidium iodide (PI) staining method. Lower left, viable cells; lower right, early apoptotic cells; upper right, late apoptotic cells; upper left, necrotic cells. (b) Histogram showing populations for HeLa cells in three stages treated by complex **3**. (c) Effect of NAC (5 mM) on induced apoptosis by complex **3**.

Cellular Localization Assay

In the process of apoptosis, cancer cells get stimuli from different intracellular organelles. Thus, apoptosis induced by Ru(II) complexes (**1**-**3**) requires a deeper understanding of their cellular targets and mechanisms.[18,35,40] Being fluorescence active (Figure S19), the subcellular localization of **1**–**3** was explored along with the commercially available staining probes such as Hoechst 33342 for the nucleus and MitoTracker Deep Red (MTDR) for mitochondria using live cell confocal microscopy colocalization studies. Further, the colocalization effect of complexes was quantified using Pearson's correlation coefficient (PCC) for both nucleus and mitochondria staining probes. So, initially, the confocal images of the compounds along with Hoechst 33342 were taken against HeLa and HT-29 cells. The

obtained PCC values of the green fluorescent signals of **1**–**3** with blue fluorescent signals of Hoechst 33342 are very poor; that is 0.10, **1**; 0.25, **2**; and 0.18, **3** against Hela cells whereas 0.26, **1**; 0.23, **2**; and 0.28, **3** against HT-29 cells. This data, therefore, specifies that the nucleus is not a preferential target of the biological action of **1**–**3** tested in this present work. The representative confocal images of **3** along with Hoechst 33342 against HeLa and HT-29 are given in Figure 13 whereas for **1**, and **2** in Figure S20 of Supporting Information.

In order to assess the actual target of **1**–**3**, another colocalization experiment was performed with standard commercially available MTDR dye. From the results, it is observed that the green fluorescence of **1**–**3** overlapped with the red fluorescence signals of MTDR, yielding the Pearson's correlation coefficients of 0.71, 0.73, and 0.75, respectively, on live HeLa cells. All the complexes exhibit characteristic colocalization (more than 70%) with MTDR allowing complexes to specifically target mitochondria. Also, the colocalization results were acquired for HT-29 cells, yielding Pearson's correlation coefficients of 0.78, 0.80, and 0.89 for **1**, **2**, and **3** respectively. From the colocalization results in HeLa and HT-29 cells, it can be stated that **1**–**3** are predominantly localized in mitochondria irrespective of the change of cancer cells. Among the series, **3** exhibited the maximum colocalization coefficient which also exhibited higher hydrophobicity and fluorescence activity as discussed earlier. The representative confocal images of complex **3** along with MTDR against HeLa and HT-29 are given in Figure 14 whereas for 1, and 2 in Figure S21 of Supporting Information. However, it is well known in the literature that, ruthenium(II) complexes preferentially target mitochondria, and also showed the potential to influence mitochondrial metabolism.[10f,15b,35] This will make it fascinating to study the mechanism of mitochondrial function when these complexes are present.

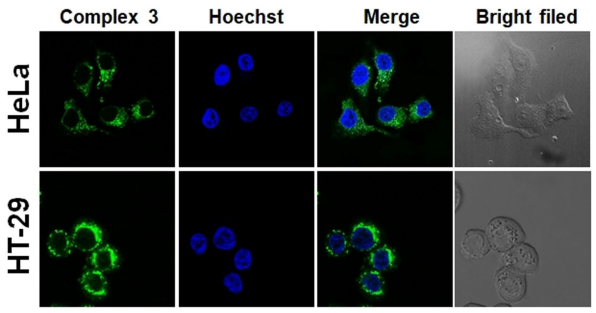

Figure 13. Confocal microscopy images of live HeLa and HT-29 cells treated with **3** (10 μM for 1 h incubation) followed by counter staining with Hoechst (0.5 μM for 5 min, stain nucleus). Hoechst, λ_{ex} = 405 nm, λ_{em} = 420–470 nm; complex, λ_{ex} = 488 nm, λ_{em} = 500–550 nm. Inset scale bars: 20 μm.

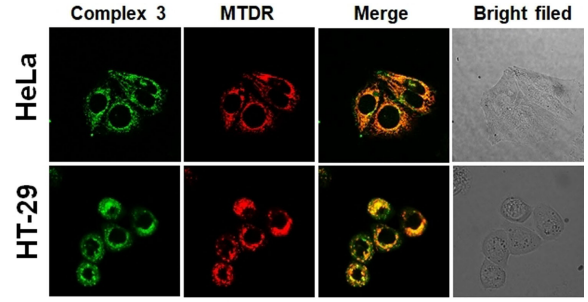

Figure 14. Confocal microscopy images of live HeLa and HT-29 cells treated with **3** (10 μM for 1 h incubation) followed by counter staining with MTDR (0.5 μM for 15 min, stain mitochondria). MTDR, λ_{ex} = 635 nm, λ_{em} = 650–740 nm; complex, λ_{ex} = 488 nm, λ_{em} = 500–550 nm. Inset scale bars: 20 μm.

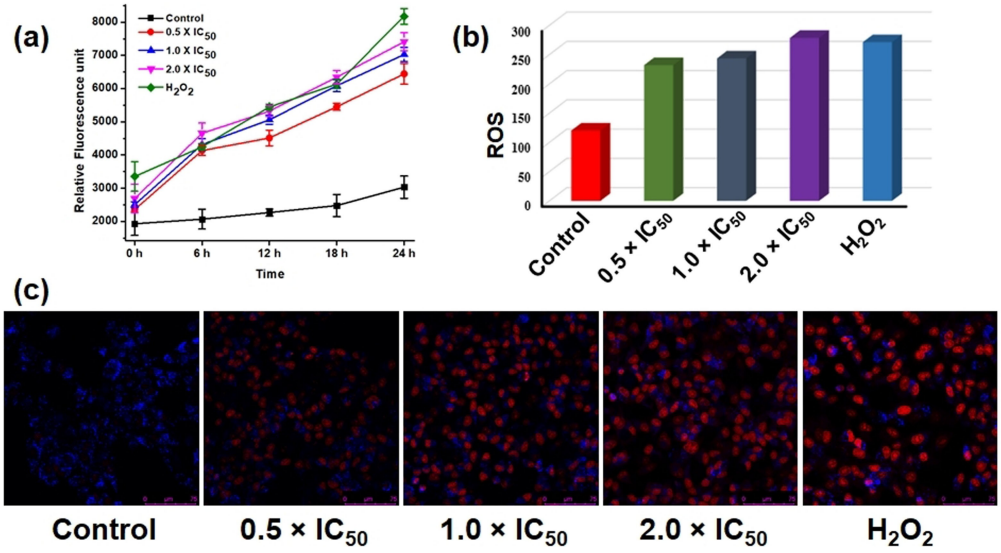

Figure 15. (a) Time dependent fluorescence kinetic measurement of ROS ($O_2^{\bullet-}$ level) generation upon treatment with **3** and DHE against HeLa cells for 24 h. **(b)** The histogram shows the level of ROS upon treatment with **3** and DHE against HeLa cells measured by flow cytometer. **(c)** Live cell confocal images of HeLa cells upon treatment with **3** and DHE; Blue channel, λ_{ex} = 405 nm, λ_{em} = 420–470 nm; red channel, λ_{ex} = 560 nm, λ_{em} = 570–640 nm.

Reactive Oxygen Species Generation Studies

From colocalization studies, **1**–**3** are found to localize at mitochondria, so the next logical step was to assess mitochondrial function or respiratory competence in the presence of these complexes. The accumulation of ROS ($O_2^{\bullet-}$ level; as mitochondria is the major contributor)[41] was investigated by staining the HeLa cells with different concentrations ($0.5\times IC_{50}$, $1.0\times IC_{50}$, $2.0\times IC_{50}$) of **3** and dihydroethidium (DHE, 5 μM) as a fluorescent probe. The results of the kinetic fluorescence (Figure 15a) and flow cytometer (Figure 15b) study showed a significant increase in ROS generation upon treatment of 3 against HeLa cells for 24 h. Confocal images (Figure 15c) suggest the increase in the red emission upon the increase in the concentrations of **3** with respect to control (blue emission). Further, the effect of NAC on ROS production was investigated by flow cytometer and confocal microscopy assays.[39] As shown in Figure S22, in presence of NAC (5 mM) the ROS generation was greatly reduced, suggesting that the increased cell fluorescence (in absence of NAC) is certainly due to the production of ROS by the **3**. Overall, the increase in ROS level may be due to the direct action of the complexes on the mitochondria, triggering mitochondrial dysfunction to produce excess ROS, leading to the induction of apoptosis.[7,15b,35,42]

Conclusion

In this study, we demonstrate the synthesis and characterization of new Ru(II) dithiocarbazate complexes with one of the most detailed investigations on biological activity highlighting their effective anticancer potential and mechanism of cell death.

In the present study, a notable instance of metal-mediated oxime-imine transformation has been reported.

The solution stability, hydrophobicity, DNA interaction, and in vitro cytotoxicity against human cancer cells HeLa, and HT-29 were performed. All complexes showed impressive cytotoxicity against both the cancer cell lines, while **3** was found to have maximum IC_{50} values of 6.9 ± 0.2 μM against HeLa cells, relatively better than the clinically used anticancer drugs cisplatin, and also some selectivity for cancer cells over healthy cells (NIH-3T3). Here, the different R-substituents present at the para-position of the aromatic ring in ligand moiety play an important role in cell cytotoxicity.

Complex **3** with high IC_{50} values was chosen for detailed analysis of cell death mechanism (apoptosis) and intracellular targets by flow cytometry and live cell imaging confocal microscopy.

Overproduction of ROS ($O_2^{\bullet-}$ level) was observed with exposure of **3** which resulting the induction of apoptosis against HeLa cells. Altogether, results suggest that **1**–**3** are potentially active to induce a mitochondrial-targeted apoptotic mode of cell death in human cancer cells. The positive outcomes from this study provide great encouragement to pursue further studies toward utilizing these ruthenium-aroyldithiocarbazoneimine complexes as anticancer agents in the near future.

Experimental Section

Benzyl chloride, 4-methylbenzyl chloride, 4-chlorobenzyl chloride, and 2,3-butanedionemonoxime were procured from Sigma Aldrich and used as received. Ruthenium trichloride was obtained from Arora Matthey. $[Ru(PPh_3)_3Cl_2]$ was synthesized from $RuCl_3$ and triphenylphosphine.[43] The solvents were dried and distilled before being used for the reaction. Reagents for biological tests were acquired mostly from Sigma-Aldrich (USA) and HiMedia laboratories.

IR spectra were recorded on a Perkin–Elmer Spectrum RXI spectrophotometer. UV-visible absorption spectra were measured on a Shimadzu spectrophotometer (UV-2450). ^{1}H and $^{13}C\{^1H\}$, and ^{31}P NMR spectra were analyzed on a Bruker Ultrashield spectrometer (400 MHz) in presence of $SiMe_4$ as the internal standard. HR-ESI-MS data were collected on a Waters XEVO G2-XS QTOF MS instrument. Fluorescence emission spectra were recorded on a Perkin Elmer LS 55 spectrofluorometer.

Synthesis of Ligands (HL^{1-3}–OH) and Complexes $[Ru^{II}(L^{1-3}–H)(PPh_3)_2Cl]$ (1–3): The synthesis and spectroscopic details of the ligands (HL^{1-3}–OH) are discussed in the Supporting Information.

$[Ru^{II}(L^1–H)(PPh_3)_2Cl]$ (1): An equimolar ratio of $[Ru(PPh_3)_3Cl_2]$ (0.1 mmol) was refluxed with HL^1–OH (0.1 mmol) in ethanol (30 mL) for 4 h. A dark green crystalline precipitate of $[Ru^{II}(L^1–H)(PPh_3)_2Cl]$ (**1**) was separated out from the reaction mixture. At room temperature, the crystals, suitable for X-ray analysis, were collected by filtration, washed with ethanol and dried in air. Yield: 0.068 g (73 %). Anal. calcd. for $C_{48}H_{44}ClN_3P_2RuS_2$ (925.48): C, 62.29; H, 4.79; N, 4.54; found C, 62.16; H, 4.86; N, 4.51. Main IR peaks (KBr, cm^{-1}): 3453 $\nu(N–H)_{imine}$, 742, 696, 515 ν(3P–Ph). UV-Vis (DMSO): λ_{max}, nm (ε, M^{-1} cm^{-1}): 478 (1448), 361 (12067). ^{1}H NMR (400 MHz, $CDCl_3$): δ (ppm) = 8.40 (s, 1H, N–H), 7.74–7.21 (m, 35H, aromatic), 3.80 (s, 2H, $-SCH_2$), 1.87–1.29 (s, 6H, $-2CH_3$). $^{13}C\{^1H\}$ NMR (100 MHz, $CDCl_3$): δ 190.74, 173.51, 152.34, 137.82–126.86 (42 C, aromatic), 39.03, 23.47, 14.72. ^{31}P NMR (120 MHz, $CDCl_3$): δ 27.32 (s, PPh_3).

$[Ru^{II}(L^2–H)(PPh_3)_2Cl]$ (2): This complex was also prepared by following the same procedure as above. Yield: 0.059 g (63 %). Anal. calcd. for $C_{49}H_{46}ClN_3P_2RuS_2$ (939.51): C, 62.64; H, 4.94; N, 4.47; Found: C, 62.55; H, 5.00; N, 4.39. Main IR Peaks (KBr pellet, cm^{-1}): 3437 $\nu(N–H)_{imine}$, 750, 697, 516 ν(3P–Ph). UV-Vis (DMSO): λ_{max}, nm (ε, M^{-1} cm^{-1}): 471 (3650), 355 (22491). ^{1}H NMR (400 MHz, $CDCl_3$): δ (ppm) = 8.40 (s, 1H, N–H), 7.75–7.04 (m, 34H, aromatic), 3.76 (s, 2H, $-SCH_2$), 2.33 (s, 3H, Ar–CH_3), 1.87–1.30 (s, 6H, $-2CH_3$). $^{13}C\{^1H\}$ NMR (100 MHz, $CDCl_3$): δ 190.86, 173.46, 152.26, 136.48–127.58 (42 C, aromatic), 38.85, 23.47, 21.13, 14.71. ^{31}P NMR (120 MHz, $CDCl_3$): δ 27.58 (s, PPh_3).

$[Ru^{II}(L^3–H)(PPh_3)_2Cl]$ (3): This complex was also prepared by following the same procedure as above. Yield: 0.056 g (59 %). Anal. calcd. for $C_{48}H_{43}Cl_2N_3P_2RuS_2$ (959.93): C, 60.06; H, 4.52; N, 4.38; Found: C, 60.13; H, 4.44; N, 4.39. Main IR Peaks (KBr pellet, cm^{-1}): 3432 $\nu(N–H)_{imine}$, 746, 699, 511 ν(3P–Ph). UV-Vis (DMSO): λ_{max}, nm (ε, M^{-1} cm^{-1}): 469 (3455), 357 (22910). ^{1}H NMR (400 MHz, $CDCl_3$): δ (ppm) = 8.41 (s, 1H, N–H), 8.12–7.05 (m, 34H, aromatic), 3.79 (s, 2H, $-SCH_2$), 1.88–1.24 (s, 6H, $-2CH_3$). $^{13}C\{^1H\}$ NMR (100 MHz, $CDCl_3$): δ 190.57, 173.59, 165.46, 136.74–127.59 (42 C, aromatic), 37.96, 29.71, 14.69. ^{31}P NMR (120 MHz, $CDCl_3$): δ 27.50 (s, PPh_3).

Single crystal X-ray Structure Determination and Biological Assays: The details of all the experimental procedures were added in the Supporting Information. Deposition Number(s) 2192720 (for **1**), 2192721 (for **2**) contain the supplementary crystallographic data for this paper. These data are provided free of charge by the joint

Cambridge Crystallographic Data Centre and Fachinformationszentrum Karlsruhe Access Structures service.

Acknowledgements

Rupam Dinda thanks CSIR, Govt. of India [Grant No. 01(3073)/21/EMR-II] for funding and also the fellowship for SD. Open Access funding enabled and organized by Projekt DEAL.

Conflict of Interest

The authors declare no conflict of interest.

Data Availability Statement

The data that support the findings of this study are available on request from the corresponding author. The data are not publicly available due to privacy or ethical restrictions.

Keywords: cytotoxicity · DNA interaction · mitochondria-mediated apoptosis · ruthenium(II)-dithiocarbazates · solution study

[1] a) R. G. Kenny, C. J. Marmion, *Chem. Rev.* **2019**, *119*, 1058–1137; b) X. Wang, X. Wang, S. Jin, N. Muhammad, Z. Guo, *Chem. Rev.* **2019**, *119*, 1138–1192; c) Pragti, B. K. Kundu, S. Mukhopadhyay, *Coord. Chem. Rev.* **2021**, *448*, 214169, 10.1016/j.ccr.2021.214169; d) V. Brabec, J. Kasparkova, *Coord. Chem. Rev.* **2018**, *376*, 75–94; e) A. Rilak Simović, R. Masnikosa, I. Bratsos, E. Alessio, *Coord. Chem. Rev.* **2019**, *398*, 113011; f) S. M. Meier-Menches, C. Gerner, W. Berger, C. G. Hartinger, B. K. Keppler, *Chem. Soc. Rev.* **2018**, *47*, 909–928; g) M. R. Gill, J. A. Thomas, *Chem. Soc. Rev.* **2012**, *41*, 3179–3192; h) L. Gourdon, K. Cariou, G. Gasser, *Chem. Soc. Rev.* **2022**, *51*, 1167–1195; i) A. Notaro, M. Jakubaszek, N. Rotthowe, F. Maschietto, R. Vinck, P. S. Felder, B. Goud, M. Tharaud, I. Ciofini, F. Bedioui, R. F. Winter, G. Gasser, *J. Am. Chem. Soc.* **2020**, *142*, 6066–6084; j) B. Englinger, C. Pirker, P. Heffeter, A. Terenzi, C. R. Kowol, B. K. Keppler, W. Berger, *Chem. Rev.* **2019**, *119*, 1519–1624.

[2] X. Yao, K. Panichpisal, N. Kurtzman, K. Nugent, *Am. J. Med. Sci.* **2007**, *334*, 115–124.

[3] a) G. H. Ribeiro, A. P. M. Guedes, T. D. de Oliveira, C. R. S. T. B. de Correia, L. Colina-Vegas, M. A. Lima, J. A. Nóbrega, M. R. Cominetti, F. V. Rocha, A. G. Ferreira, E. E. Castellano, F. R. Teixeira, A. A. Batista, *Inorg. Chem.* **2020**, *59*, 15004–15018; b) N. Alatrash, F. H. Issa, N. S. Bawazir, S. J. West, K. E. van Manen-Brush, C. P. Shelor, A. S. Dayoub, K. A. Myers, C. Janetopoulos, E. A. Lewis, *Chem. Sci.* **2020**, *11*, 264–275; c) M. Piccolo, G. Misso, M. G. Ferraro, C. Riccardi, A. Capuozzo, M. R. Zarone, F. Maione, M. Trifuoggi, P. Stiuso, G. D'Errico, *Sci. Rep.* **2019**, *9*, 1–15.

[4] J. M. Rademaker-Lakhai, D. van den Bongard, D. Pluim, J. H. Beijnen, J. H. M. Schellens, *Clin. Cancer Res.* **2004**, *10*, 3717–3727.

[5] C. G. Hartinger, M. A. Jakupec, S. Zorbas-Seifried, M. Groessl, A. Egger, W. Berger, H. Zorbas, P. J. Dyson, B. K. Keppler, *Chem. Biodiversity* **2008**, *5*, 2140–2155.

[6] R. Trondl, P. Heffeter, C. R. Kowol, M. A. Jakupec, W. Berger, B. K. Keppler, *Chem. Sci.* **2014**, *5*, 2925–2932.

[7] S. Thota, D. A. Rodrigues, D. C. Crans, E. J. Barreiro, *J. Med. Chem.* **2018**, *61*, 5805–5821.

[8] a) C. Scolaro, A. Bergamo, L. Brescacin, R. Delfino, M. Cocchietto, G. Laurenczy, T. J. Geldbach, G. Sava, P. J. Dyson, *J. Med. Chem.* **2005**, *48*, 4161–4171; b) C. A. Vock, C. Scolaro, A. D. Phillips, R. Scopelliti, G. Sava, P. J. Dyson, *J. Med. Chem.* **2006**, *49*, 5552–5561.

[9] R. E. Aird, J. Cummings, A. A. Ritchie, M. Muir, R. E. Morris, H. Chen, P. J. Sadler, D. Jodrell, *Br. J. Cancer* **2002**, *86*, 1652–1657.

[10] a) A. Notaro, M. Jakubaszek, S. Koch, R. Rubbiani, O. Dömötör, É. A. Enyedy, M. Dotou, F. Bedioui, M. Tharaud, B. Goud, S. Ferrari, E. Alessio, G. Gasser, *Chem.* **2020**, *26*, 4997–5009; b) A.-C. Munteanu, A. Notaro, M. Jakubaszek, J. Cowell, M. Tharaud, B. Goud, V. Uivarosi, G. Gasser, *Inorg. Chem.* **2020**, *59*, 4424–4434; c) A. Notaro, A. Frei, R. Rubbiani, M. Jakubaszek, U. Basu, S. Koch, C. Mari, M. Dotou, O. Blacque, J. Gouyon, F. Bedioui, N. Rotthowe, R. F. Winter, B. Goud, S. Ferrari, M. Tharaud, M. Řezáčová, J. Humajová, P. Tomšík, G. Gasser, *J. Med. Chem.* **2020**, *63*, 5568–5584; d) N. Soliman, G. Gasser, C. M. Thomas, *Adv. Mater.* **2020**, *32*, e2003294; e) H.-L. Huang, Z.-Z. Li, Z.-H. Liang, J.-H. Yao, Y.-J. Liu, *Eur. J. Med. Chem.* **2011**, *46*, 3282–3290; f) C.-C. Zeng, S.-H. Lai, J.-H. Yao, C. Zhang, H. Yin, W. Li, B.-J. Han, Y.-J. Liu, *Eur. J. Med. Chem.* **2016**, *122*, 118–126; g) H. Huang, P. Zhang, B. Yu, Y. Chen, J. Wang, L. Ji, H. Chao, *J. Med. Chem.* **2014**, *57*, 8971–8983; h) N. Alatrash, E. S. Narh, A. Yadav, M.-J. Kim, T. Janaratne, J. Gabriel, F. M. MacDonnell, *ChemMedChem* **2017**, *12*, 1055–1069; i) P. G. Nandi, P. K. Jadi, K. Das, S. J. Prathapa, B. B. Mandal, A. Kumar, *Inorg. Chem.* **2021**, *60*, 7422–7432.

[11] a) M.-G. Mendoza-Ferri, C. G. Hartinger, R. E. Eichinger, N. Stolyarova, K. Severin, M. A. Jakupec, A. A. Nazarov, B. K. Keppler, *Organometallics* **2008**, *27*, 2405–2407; b) M. G. Mendoza-Ferri, C. G. Hartinger, M. A. Mendoza, M. Groessl, A. E. Egger, R. E. Eichinger, J. B. Mangrum, N. P. Farrell, M. Maruszak, P. J. Bednarski, F. Klein, M. A. Jakupec, A. A. Nazarov, K. Severin, B. K. Keppler, *J. Med. Chem.* **2009**, *52*, 916–925; c) A. Kurzwernhart, W. Kandioller, S. Bächler, C. Bartel, S. Martic, M. Buczkowska, G. Mühlgassner, M. A. Jakupec, H.-B. Kraatz, P. J. Bednarski, V. B. Arion, D. Marko, B. K. Keppler, C. G. Hartinger, *J. Med. Chem.* **2012**, *55*, 10512–10522; d) W. F. Schmid, R. O. John, V. B. Arion, M. A. Jakupec, B. K. Keppler, *Organometallics* **2007**, *26*, 6643–6652; e) W. Ginzinger, G. Mühlgassner, V. B. Arion, M. A. Jakupec, A. Roller, M. S. Galanski, M. Reithofer, W. Berger, B. K. Keppler, *J. Med. Chem.* **2012**, *55*, 3398–3413; f) P. Srivastava, M. Verma, A. Kumar, P. Srivastava, R. Mishra, S. Sivakumar, A. K. Patra, *Dalton Trans.* **2021**, *50*, 3629–3640; g) S. Swaminathan, J. Haribabu, M. K. Mohamed Subarkhan, D. Gayathri, N. Balakrishnan, N. Bhuvanesh, C. Echeverria, R. Karvembu, *Dalton Trans.* **2021**, *50*, 16311–16325; h) J. Haribabu, G. Sabapathi, M. M. Tamizh, C. Balachandran, N. S. P. Bhuvanesh, P. Venuvanalingam, R. Karvembu, *Organometallics* **2018**, *37*, 1242–1257; i) R. E. Morris, R. E. Aird, P. d S Murdoch, H. Chen, J. Cummings, N. D. Hughes, S. Parsons, A. Parkin, G. Boyd, D. I. Jodrell, P. J. Sadler, *J. Med. Chem.* **2001**, *44*, 3616–3621; j) A. Habtemariam, M. Melchart, R. Fernandez, S. Parsons, I. D. H. Oswald, A. Parkin, F. P. A. Fabbiani, J. E. Davidson, A. Dawson, R. E. Aird, D. I. Jodrell, P. J. Sadler, *J. Med. Chem.* **2006**, *49*, 6858–6868; k) N. R. Palepu, S. L. Nongbri, J. R. Premkumar, A. K. Verma, K. Bhattacharjee, S. R. Joshi, S. Forbes, Y. Mozharivskyj, R. Thounaojam, K. Aguan, M. R. Kollipara, *J. Biol. Inorg. Chem.* **2015**, *20*, 619–638; l) N. Roy, U. Sen, Y. Madaan, V. Muthukumar, S. Varddhan, S. K. Sahoo, D. Panda, B. Bose, P. Paira, *Inorg. Chem.* **2020**, *59*, 17689–17711; m) R. P. Paitandi, V. Sharma, V. D. Singh, B. K. Dwivedi, S. M. Mobin, D. S. Pandey, *Dalton Trans.* **2018**, *47*, 17500–17514; n) M. Maji, S. Acharya, I. Bhattacharya, A. Gupta, A. Mukherjee, *Inorg. Chem.* **2021**, *60*, 4744–4754; o) R. Chatterjee, I. Bhattacharya, S. Roy, K. Purkait, T. S. Koley, A. Gupta, A. Mukherjee, *Inorg. Chem.* **2021**, *60*, 12172–12185; p) S. K. Tripathy, U. De, N. Dehury, S. Pal, H. S. Kim, S. Patra, *Dalton Trans.* **2014**, *43*, 14546–14549; q) B. Mohan, S. Estalayo-Adrián, D. Umadevi, B. La Cour Poulsen, S. Blasco, G. J. McManus, T. Gunnlaugsson, S. Shanmugaraju, *Inorg. Chem.* **2022**, *61*, 11592–11599.

[12] a) M. R. Maurya, A. Kumar, A. R. Bhat, A. Azam, C. Bader, D. Rehder, *Inorg. Chem.* **2006**, *45*, 1260–1269; b) M. R. Maurya, S. Khurana, Shailendra, A. Azam, W. Zhang, D. Rehder, *Eur. J. Inorg. Chem.* **2003**, *2003*, 1966–1973, 10.1002/ejic.200200642; c) M. L. Low, G. Paulus, P. Dorlet, R. Guillot, R. Rosli, N. Delsuc, K. A. Crouse, C. Policar, *BioMetals* **2015**, *28*, 553–566; d) P. I. d S Maia, A. G. d A Fernandes, J. J. N. Silva, A. D. Andricopulo, S. S. Lemos, E. S. Lang, U. Abram, V. M. Deflon, *J. Inorg. Biochem.* **2010**, *104*, 1276–1282; e) B. Neelam, M. Mannar R, N. Fehmida, B. Alok, B. Sudha, A. Amir, *Eur. J. Med. Chem.* **2000**, *35*, 481–486; f) P. Kalaivani, R. Prabhakaran, E. Vaishnavi, T. Rueffer, H. Lang, P. Poornima, R. Renganathan, V. Vijaya Padma, K. Natarajan, *Inorg. Chem. Front.* **2014**, *1*, 311; g) M. L. Low, L. Maigre, P. Dorlet, R. Guillot, J.-M. Pagès, K. A. Crouse, C. Policar, N. Delsuc, *Bioconjugate Chem.* **2014**, *25*, 2269–2284; h) M. L. Low, L. Maigre, M. I. M. Tahir, E. R. T. Tiekink, P. Dorlet, R. Guillot, T. B. Ravoof, R. Rosli, J.-M. Pagès, C. Policar, N. Delsuc, K. A. Crouse, *Eur. J. Med. Chem.* **2016**, *120*, 1–12; i) P. Vijayan, P. Viswanathamurthi, P. Sugumar, M. N. Ponnuswamy, M. D. Balakumaran, P. T. Kalaichelvan, K. Velmurugan, R. Nandhakumar, R. J. Butcher, *Inorg. Chem. Front.* **2015**, *2*, 620–639; j) M. X. Li, L. Z. Zhang, C. L. Chen, J. Y. Niu, B. S. Ji, *J. Inorg. Biochem.* **2012**, *106*, 117–125.

[13] a) C. d Q O Cavalcante, D. d S Arcanjo, G. G. d Silva, D. M. de Oliveira, C. C. Gatto, *New J. Chem.* **2019**, *43*, 11209–11221; b) S. A. Elsayed, H. E. Badr, A. Di Biase, A. M. El-Hendawy, *J. Inorg. Biochem.* **2021**, *223*, 111549; c) A. M. Sarhan, S. A. Elsayed, M. M. Mashaly, A. M. El-Hendawy, *Appl. Organomet. Chem.* **2019**, *33*, e4655; d) W. P. Sohtun, T. Khamrang, A. Kannan, G. Balakrishnan, D. Saravanan, M. A. Akhbarsha, M. Velusamy, M. Palaniandavar, *Appl. Organomet. Chem.* **2020**, *34*; e) Z. Yekkeghasemi, M. Ramezani, J. T. Mague, R. Takjoo, *New J. Chem.* **2020**, *44*, 8878–8889; f) R. Zahan, M. S. Rahi, M. C. Sheikh, R. Miyatake, E. Zangrando, T. Naz, M. A.-A.-A.-A. Islam, M. A. Reza, *Appl. Organomet. Chem.* **2019**, *33*, e4601.

[14] a) Y. Gou, X. Jia, L. X. Hou, J. G. Deng, G. J. Huang, H. W. Jiang, F. Yang, *J. Med. Chem.* **2022**, *65*, 6677–6689; b) Y. Gou, M. Chen, S. Li, J. Deng, J. Li, G. Fang, F. Yang, G. Huang, *J. Med. Chem.* **2021**, *64*, 5485–5499.

[15] a) Q. Du, Y. Yang, L. Guo, M. Tian, X. Ge, Z. Tian, L. Zhao, Z. Xu, J. Li, Z. Liu, *Dyes Pigm.* **2019**, *162*, 821–830; b) K. Wang, C. Zhu, Y. He, Z. Zhang, W. Zhou, N. Muhammad, Y. Guo, X. Wang, Z. Guo, *Angew. Chem. Int. Ed. Engl.* **2019**, *58*, 4638–4643; c) A. Castonguay, C. Doucet, M. Juhas, D. Maysinger, *J. Med. Chem.* **2012**, *55*, 8799–8806; d) S. Jin, Y. Hao, Z. Zhu, N. Muhammad, Z. Zhang, K. Wang, Y. Guo, Z. Guo, X. Wang, *Inorg. Chem.* **2018**, *57*, 11135–11145.

[16] S. Roy, M. Mohanty, R. G. Miller, S. A. Patra, S. Lima, A. Banerjee, N. Metzler-Nolte, E. Sinn, W. Kaminsky, R. Dinda, *Inorg. Chem.* **2020**, *59*, 15526–15540.

[17] a) G. Sahu, S. A. Patra, M. Mohanty, S. Lima, P. D. Pattanayak, W. Kaminsky, R. Dinda, *J. Inorg. Biochem.* **2022**, *233*, 111844; b) A. Banerjee, M. Mohanty, S. Lima, R. Samanta, E. Garribba, T. Sasamori, R. Dinda, *New J. Chem.* **2020**, *44*, 10946–10963.

[18] J. Li, L. Guo, Z. Tian, S. Zhang, Z. Xu, Y. Han, R. Li, Y. Li, Z. Liu, *Inorg. Chem.* **2018**, *57*, 13552–13563.

[19] Z. Zhao, Z. Luo, Q. Wu, W. Zheng, Y. Feng, T. Chen, *Dalton Trans.* **2014**, *43*, 17017–17028.

[20] V. Pierroz, T. Joshi, A. Leonidova, C. Mari, J. Schur, I. Ott, L. Spiccia, S. Ferrari, G. Gasser, *J. Am. Chem. Soc.* **2012**, *134*, 20376–20387.

[21] a) A. Banerjee, S. P. Dash, M. Mohanty, G. Sahu, G. Sciortino, E. Garribba, M. F. N. N. Carvalho, F. Marques, J. Costa Pessoa, W. Kaminsky, K. Brzezinski, R. Dinda, *Inorg. Chem.* **2020**, *59*, 14042–14057; b) M. Mohanty, G. Sahu, A. Banerjee, S. Lima, S. A. Patra, A. Crochet, G. Sciortino, D. Sanna, V. Ugone, E. Garribba, R. Dinda, *Inorg. Chem.* **2022**, *61*, 4513–4532; c) S. A. Patra, A. Banerjee, G. Sahu, M. Mohanty, S. Lima, D. Mohapatra, H. Görls, W. Plass, R. Dinda, *J. Inorg. Biochem.* **2022**, *233*, 111852; d) G. Sahu, A. Banerjee, R. Samanta, M. Mohanty, S. Lima, E. R. T. Tiekink, R. Dinda, *Inorg. Chem.* **2021**, *60*, 15291–15309; e) Saswati, P. Adão, S. Majumder, S. P. Dash, S. Roy, M. L. Kuznetsov, J. Costa Pessoa, C. S. B. Gomes, M. R. Hardikar, E. R. T. Tiekink, R. Dinda, *Dalton Trans.* **2018**, *47*, 11358–11374, 10.1039/C8DT01668B; f) S. Roy, M. Böhme, S. P. Dash, M. Mohanty, A. Buchholz, W. Plass, S. Majumder, S. Kulanthaivel, I. Banerjee, H. Reuter, W. Kaminsky, R. Dinda, *Inorg. Chem.* **2018**, *57*, 5767–5781; g) S. P. Dash, A. K. Panda, S. Pasayat, R. Dinda, A. Biswas, E. R. T. Tiekink, S. Mukhopadhyay, S. K. Bhutia, W. Kaminsky, E. Sinn, *RSC Adv.* **2015**, *5*, 51852–51867; h) S. Lima, A. Banerjee, M. Mohanty, G. Sahu, C. Kausar, S. K. Patra, E. Garribba, W. Kaminsky, R. Dinda, *New J. Chem.* **2019**, *43*, 17711–17725; i) S. P. Dash, S. Pasayat, S. Bhakat, S. Roy, R. Dinda, E. R. T. Tiekink, S. Mukhopadhyay, S. K. Bhutia, M. R. Hardikar, B. N. Joshi, Y. P. Patil, M. Nethaji, *Inorg. Chem.* **2013**, *52*, 14096–14107; j) S. P. Dash, A. K. Panda, S. Pasayat, S. Majumder, A. Biswas, W. Kaminsky, S. Mukhopadhyay, S. K. Bhutia, R. Dinda, *J. Inorg. Biochem.* **2015**, *144*, 1–12; k) S. P. Dash, A. K. Panda, S. Pasayat, R. Dinda, A. Biswas, E. R. T. Tiekink, Y. P. Patil, M. Nethaji, W. Kaminsky, S. Mukhopadhyay, S. K. Bhutia, *Dalton Trans.* **2014**, *43*, 10139–10156; l) M. Mohanty, S. K. Maurya, A. Banerjee, S. A. Patra, M. R. Maurya, A. Crochet, K. Brzezinski, R. Dinda, *New J. Chem.* **2019**, *43*, 17680–17695; m) Saswati, M. Mohanty, A. Banerjee, S. Biswal, A. Horn, G. Schenk, K. Brzezinski, E. Sinn, H. Reuter, R. Dinda, *J. Inorg. Biochem.* **2020**, *203*, 110908, 10.1016/j.jinorgbio.2019.110908; n) S. A. Patra, M. Mohanty, A. Banerjee, S. Kesarwani, F. Henkel, H. Reuter, R. Dinda, *J. Inorg. Biochem.* **2021**, *224*, 111582; o) S. Roy, M. Böhme, S. Lima, M. Mohanty, A. Banerjee, A. Buchholz, W. Plass, S. Rathnam, I. Banerjee, W. Kaminsky, R. Dinda, *Eur. J. Inorg. Chem.* **2022**, *2022*; p) S. Roy, M. Mohanty, S. Pasayat, S. Majumder, K. Senthilguru, I. Banerjee, M. Reichelt, H. Reuter, E. Sinn, R. Dinda, *J. Inorg. Biochem.* **2017**, *172*, 110–121; q) S. Lima, A. Banerjee, G. Sahu, S. A. Patra, K. Sahu, T. Sasamori, G. Sciortino, E. Garribba, R. Dinda, *J. Inorg. Biochem.* **2022**, *233*, 111853.

[22] a) A. B. Beshir, S. K. Guchhait, J. A. Gascón, G. Fenteany, *Bioorg. Med. Chem. Lett.* **2008**, *18*, 498–504; b) R. A. Peralta, A. J. Bortoluzzi, B. de Souza, R. Jovito, F. R. Xavier, R. A. A. Couto, A. Casellato, F. Nome, A. Dick, L. R. Gahan, G. Schenk, G. R. Hanson, F. C. S. de Paula, E. C. Pereira-Maia, S. de P Machado, P. C. Severino, C. Pich, T. Bortolotto, H. Terenzi, E. E. Castellano, A. Neves, M. J. Riley, *Inorg. Chem.* **2010**, *49*, 11421–11438; c) A. Bolognese, G. Correale, M. Manfra, A. Lavecchia, O. Mazzoni, E. Novellino, V. Barone, P. La Colla, R. Loddo, *J. Med. Chem.* **2002**, *45*, 5217–5223; d) V. Sharma, A. Chaudhary, S. Arora, A. K. Saxena, M. P. S. Ishar, *Eur. J. Med. Chem.* **2013**, *69*, 310–315.

[23] a) A. K. Das, S.-M. Peng, S. Bhattacharya, *J. Chem. Soc. Dalton Trans.* **2000**, 181–184, 10.1039/A907021D; b) S. K. Singh, S. Sharma, S. D. Dwivedi, R.-Q. Zou, Q. Xu, D. S. Pandey, *Inorg. Chem.* **2008**, *47*, 11942–11949.

[24] I. Chakraborty, B. K. Panda, J. Gangopadhyay, A. Chakravorty, *Inorg. Chem.* **2005**, *44*, 1054–1060.

[25] V. Y. Kukushkin, T. Nishioka, D. Tudela, K. Isobe, I. Kinoshita, *Inorg. Chem.* **1997**, *36*, 6157–6165.

[26] S. Naskar, D. Mishra, R. J. Butcher, S. K. Chattopadhyay, *Polyhedron* **2007**, *26*, 3703–3714.

[27] L. Biancalana, L. K. Batchelor, T. Funaioli, S. Zacchini, M. Bortoluzzi, G. Pampaloni, P. J. Dyson, F. Marchetti, *Inorg. Chem.* **2018**, *57*, 6669–6685.

[28] C. A. Puckett, R. J. Ernst, J. K. Barton, *Dalton Trans.* **2010**, *39*, 1159–1170.

[29] N. C. Desai, N. Bhatt, H. Somani, A. Trivedi, *Eur. J. Med. Chem.* **2013**, *67*, 54–59.

[30] D. Sun, Y. Liu, D. Liu, R. Zhang, X. Yang, J. Liu, *Chem.* **2012**, *18*, 4285–4295.

[31] K. Benner, H. Ihmels, S. Kölsch, P. M. Pithan, *Org. Biomol. Chem.* **2014**, *12*, 1725–1734.

[32] Z. Afsan, T. Roisnel, S. Tabassum, F. Arjmand, *Bioorg. Chem.* **2020**, *94*, 103427.

[33] a) J. D. Aguirre, A. M. Angeles-Boza, A. Chouai, C. Turro, J.-P. Pellois, K. R. Dunbar, *Dalton Trans.* **2009**, 10806–10812, 10.1039/B915357H; b) S. H. van Rijt, A. Mukherjee, A. M. Pizarro, P. J. Sadler, *J. Med. Chem.* **2010**, *53*, 840–849; c) G. Agonigi, L. Biancalana, M. G. Lupo, M. Montopoli, N. Ferri, S. Zacchini, F. Binacchi, T. Biver, B. Campanella, G. Pampaloni, V. Zanotti, F. Marchetti, *Organometallics* **2020**, *39*, 645–657.

[34] K.-J. Du, J.-Q. Wang, J.-F. Kou, G.-Y. Li, L.-L. Wang, H. Chao, L.-N. Ji, *Eur. J. Med. Chem.* **2011**, *46*, 1056–1065.

[35] W. Ma, S. Zhang, Z. Tian, Z. Xu, Y. Zhang, X. Xia, X. Chen, Z. Liu, *Eur. J. Med. Chem.* **2019**, *181*, 111599.

[36] S. W. Chang, A. R. Lewis, K. E. Prosser, J. R. Thompson, M. Gladkikh, M. B. Bally, J. J. Warren, C. J. Walsby, *Inorg. Chem.* **2016**, *55*, 4850–4863.

[37] a) S. Balaji, M. K. Mohamed Subarkhan, R. Ramesh, H. Wang, D. Semeril, *Organometallics* **2020**, *39*, 1366–1375; b) Z. Tian, Y. Yang, L. Guo, G. Zhong, J. Li, Z. Liu, *Inorg. Chem. Front.* **2018**, *5*, 3106–3112.

[38] Y. H. Han, S. H. Kim, S. Z. Kim, W. H. Park, *Life Sci.* **2008**, *83*, 346–355.

[39] a) J. Zhao, S. Li, X. Wang, G. Xu, S. Gou, *Inorg. Chem.* **2019**, *58*, 2208–2217; b) A. Ferino, G. Nicoletto, F. D'Este, S. Zorzet, S. Lago, S. N. Richter, A. Tikhomirov, A. Shchekotikhin, L. E. Xodo, *J. Med. Chem.* **2020**, *63*, 1245–1260.

[40] Z. Tian, J. Li, S. Zhang, Z. Xu, Y. Yang, D. Kong, H. Zhang, X. Ge, J. Zhang, Z. Liu, *Inorg. Chem.* **2018**, *57*, 10498–10502.

[41] V. G. Grivennikova, A. D. Vinogradov, *Biochim. Biophys. Acta* **2006**, *1757*, 553–561.

[42] C. Pérez-Arnaiz, M. I. Acuña, N. Busto, I. Echevarría, M. Martínez-Alonso, G. Espino, B. García, F. Domínguez, *Eur. J. Med. Chem.* **2018**, *157*, 279–293.

[43] P. S. Hallman, T. A. Stephenson, G. Wilkinson, *Inorg. Synth.* **1970**, *12*, 237–240.

Manuscript received: August 29, 2022
Accepted manuscript online: January 4, 2023
Version of record online: February 24, 2023